AIAA Propulsion and Energy Forum
19-22 August 2019, Indianapolis, IN
AIAA Propulsion and Energy 2019 Forum

10.2514/6.2019-4076

Frequency Scaling of the Hall Thruster Breathing Mode

Ethan T. Dale * and Benjamin A. Jorns†
University of Michigan, Ann Arbor, MI 48109

The scaling of the breathing mode frequency in a Hall thruster predicted by several extant theoretical models is investigated. The breathing mode has been observed consistently in experiments but there is still no intuitive and experimentally-validated analytical model for its onset and growth. A simple way to evaluate proposed mechanisms for this instability is to compare the predicted real frequency trends with those observed experimentally. A combination of laser and electrostatic diagnostics are employed to determine a wide range of plasma and neutral parameters needed to perform this comparison. In particular, the one-dimensional Boltzmann equation for ions is used to infer quantities like the electric field strength and ionization frequency using velocity moments measured with laser-induced fluorescence. Using this information, the predator-prey model, resistive instability, and a neutral gas instability are considered. The frequencies predicted by the predator-prey model were found not to correlate with the measured values, having either 18% or 69% null confidence. For the resistive instability, positive correlation between predicted and observed frequencies existed only in the vicinity of the ionization and acceleration regions, but the relationship again was statistically insignificant with between 20% and 60% null confidence. Finally, a neutral-driven instability was explored by considering the neutral transit and acoustic frequencies. The former did not correlate positively while the latter did, but uncertainty in the neutral sound speed suggests this trend is insignificant. In total, none of the three hypotheses explored are found to be consistent with experimental breathing frequency trends. These results are discussed in the context of alternative mechanisms for the breathing mode.

Nomenclature

c	=	speed of light in vacuum, m/s
e	=	fundamental charge, C
E_z	=	axial electric field strength, V/m
f_{iz}	=	ionization frequency, Hz
f_n	=	plasma density gradient frequency, Hz
j_i	=	ion current density, A m^{-2}
k	=	wavenumber, m^{-1}
L	=	length scale, m
m_i	=	ion mass, kg
n	=	plasma density, m^{-3}
N	=	number of samples
n_n	=	neutral density, m^{-3}
r	=	correlation coefficient
t	=	time, s
T_i	=	ion temperature, eV
T_n	=	neutral temperature, K
u_i	=	ion velocity, m/s
u_n	=	neutral gas velocity, m/s
z	=	axial position, m
γ	=	growth rate, rad/s
δ	=	resistive factor

*PhD Candidate, Department of Aerospace Engineering, AIAA Member
†Assistant Professor and Co-Director of Plasmadynamics and Electric Propulsion Laboratory, Department of Aerospace Engineering, AIAA Senior Member

λ	=	wavelength, m
λ_0	=	nominal wavelength, m
μ_e	=	electron mobility, C s kg^{-1}
σ	=	standard deviation
ω_b	=	breathing frequency, rad/s
ω_r	=	real frequency, rad/s

I. Introduction

Hall thrusters are an electric propulsion technology that utilize crossed static electric and magnetic fields to generate and accelerate a plasma for the purpose of producing thrust. These systems are enabling for in-space propulsion, offering high specific impulse combined with moderate thrust density. These advantages have led to their increasingly widespread use for applications ranging from stationkeeping to deep space missions.[1] With that said, there are a number of outstanding technical challenges related to the development and integration of this technology. One of the most notable is related to stability: these devices host a wide variety of plasma and electrical oscillations that can greatly hamper the performance or lifetime of the thruster. Since the performance of any space propulsion system must be reliable and repeatable to guarantee that it will operate successfully outside of a laboratory setting, the stability of the Hall thruster discharge is of utmost importance when designing and flying these devices. Conversely, the presence of destabilizing processes requires thorough examination and, if necessary, mitigation.

A major phenomenon influencing stability that has been studied extensively is the existence of low-frequency discharge current oscillations, colloquially called the "breathing mode".[2] This oscillation is universal in Hall thrusters, with observations reported in a wide variety of systems over the decades. Further, studies have shown that it corresponds with changes in performance and is linked to life-limiting thruster erosion processes.[3, 4] Given the importance and ubiquity of this instability, there have been a number of attempts to understand its origin. Proposed theories include a predator-prey process, a resistive instability, and a neutral gas instability. While these disparate hypotheses in many cases have yielded predictions for breathing mode frequencies that are commensurate with measured values, there is yet to be a theory that is both widely accepted and validated experimentally.[5–8] This is a critical missing gap in the understanding of thrusters as the insight gained from a validated theory would be invaluable for differentiating stable from unstable operating conditions, and possibly shedding light on mitigation techniques.

The lack of validation to date stems primarily from the challenges in experimental testing of the underlying assumptions and predictions for many of the proposed mechanisms for the breathing mode. Indeed, there are several major plasma properties inside the thruster discharge channel that must be measured to validate a theory, but accessing this region of a thruster non-invasively and meaningfully has proved to be technically prohibitive. As a consequence, it has not been possible to directly rule out or confirm many of the oscillation mechanisms that have been proposed. Given the importance of the breathing mode and understanding its origin to Hall thruster development, there thus remains a pressing need to perform these experimental assessments.

The goal of this paper is to apply recent advances in data analysis and diagnostic techniques to attempt to generate the data necessary to perform detailed validation of many of the leading theories for the breathing mode. To that end, this paper is organized in the following way. In Section II we overview three leading proposed mechanisms for the breathing mode. In Section III, the methodology for evaluating these theories is described, including the experimental setup and analysis techniques. The results of the experiment are presented in Section IV, followed by a discussion of them in Section V. Finally in Section VI, conclusions are drawn regarding each examined breathing mode hypothesis.

II. Background

We describe in the following three of the leading proposed physical processes for the breathing mode oscillation. We review qualitatively the physical principles underlying each mode and identify key predictions for each that can be experimentally tested.

A. Predator-Prey

One of the first quantitative theories for the breathing mode was proposed by Fife et al. to accompany hybrid particle-in-cell numerical results that resolved low-frequency oscillations.[5] In that work, Fife attributed this instability to a predator-prey process in which neutral particles (prey) slowly fill the thruster channel until they are depleted by electrons (predators), at which point the cycle restarts. Fife derived a simple expression for the real oscillation frequency ω_r based on zero-dimensional neutral and ion continuity equations:

$$\omega_r = \frac{\sqrt{u_i u_n}}{L} \ , \tag{1}$$

where u_i is the ion speed, u_n is the neutral speed, and L is the characteristic length.

B. Resistive Instability

It also has been proposed that the breathing mode may be attributed to a resistive instability, which downplays the role of ionization as a growth mechanism. Although first derived as an azimuthal wave in Hall thrusters by Litvak et al.,[9] Chables and Rogier derived it axially and related it to the breathing mode.[6] In their kinetic derivation, they suggest that a Buneman instability exists that drives low-frequency oscillations. Specifically, there is a modified two-stream instability between electrons and ions that bolsters the axial electric field. Eventually the electric field collapses once the neutral gas is depleted due to enhanced ionization, but the process restarts as the neutral gas fills back in. They derived the following dispersion relation:

$$\frac{\omega}{k u_i} = -\frac{i}{2\delta} + 1 \pm \sqrt{-\frac{1}{4\delta^2} - \frac{i}{\delta}} \ , \tag{2}$$

where $\delta \equiv \frac{m_i}{e} k u_i \mu_e$, and m_i is ion mass, k is wavenumber, and μ_e is electron mobility. A similar resistive process derived solely from fluid equations by Koshkarov et al. yielded an equivalent result, although they identified a lag between ion and electron current as being a significant factor.[10]

C. Neutral Gas

The neutral gas population in a Hall thruster is often assumed to play a minor role in the dynamics of the plasma: the particles are heavy, cold, and only somewhat collisional, transitioning between continuum and free molecular flow.[11] However, the time scale of neutral transit throughout the thruster is not too far from that of the breathing mode, which opens the possibility for a neutral-driven origin of the instability. Numerical experiments have shown that low-frequency oscillations are sensitive to neutral gas properties[12], but there is limited study into the time-dependent nature of this population. Preliminary laser measurements of neutral xenon in a thruster showed little fluctuation over time.[13] However, there are a host of gas dynamic processes that could potentially be supported in a Hall thruster. For example, a thermoacoustic instability[14] might involve the presence of a neutral standing sound wave that has an anti-node located near the acceleration region; energy transfer from the plasma to the neutral gas in phase with the acoustic wave can lead to growth. Although there is little theoretical support in the literature for such an instability, let alone one that relates to the breathing mode, it remains an attractive explanation due to its simplicity.

D. Summary

To determine which breathing mode mechanism is dominant, the scaling of the real frequency can be compared to experimental measurements. That is, the trend in ω_r predicted by a given theory will be compared to that observed experimentally. The correlation between the two may be: positive, the given theory is accurate; negative, the given theory is inaccurate; or absent, the instability is not present or the measurements are simply not sensitive enough. To do this, a multitude of plasma and neutral properties must be known so as to calculate ω_r according to each theory. In particular, the predator-prey model requires u_i, u_n, and L, where these former two are average quantities in the channel. The last quantity L is poorly defined but is often approximated as the channel length, although another physically reasonable value to use is the combined width of the ionization and acceleration regions. The resistive instability additionally requires μ_e, and thus E_z and u_e. The latter can be approximated as $u_e = j_e/n \approx I_d/(A_p n) - u_i$, where I_d is the discharge current and A_b is the cross-sectional area of the plasma. We estimate this area assuming a Lorentzian current distribution in the near plume to approximate the log-triangular shape typical of measured ion current density profiles.[15] In this case k may be similar to $2\pi/L$ where L is close to the channel length – again vaguely defined. Finally, since there is no quantitative theory for a neutral instability, it may be sufficient to determine the neutral density n_n, u_n, and the neutral temperature T_n, with which we can estimate the continuum sound speed c_n.

In summary, the following quantities are required: u_i, u_n, f_{iz}, E_z, n, n_n, and T_n. The next section will describe how and under what conditions these quantities were measured.

III. Methodology

In this section, we review the practical aspects of examining the scaling laws implied by the three mechanisms previously presented. These include the facility and thruster with which the experiment was conducted and the diagnostics used to determine the quantities identified in the preceding section.

A. Facility and Thruster

Experiments were carried out at the University of Michigan in the Large Vacuum Test Facility (LVTF), a 6-m diameter by 9-m long stainless steel-clad vacuum vessel. It has thirteen LN_2-baffled cryogenic pumps and five cryosails, producing a pumping speed of roughly 575 kL/s on xenon. This allowed for typical operating pressures of $\sim 10^{-6}$ Torr-Xe.The article under test was a 9-kW magnetically-shielded Hall thruster developed by the Jet Propulsion Laboratory in collaboration with the the Air Force Research Laboratory and the University of Michigan, and described thoroughly in Refs. 16 and 17. The thruster was operated at 300 V, 15 A with five different cathode flow fractions (CFFs) to induce changes in the breathing frequency without altering the magnetic field topography or discharge voltage. The cathode was mounted above the thruster. An ionization gauge was mounted in the center exit plane of the thruster approximately 1 m away.[18] Figure 1 shows the thruster in its test configuration.

Fig. 1 The thruster under test installed in the LVTF.

B. Laser-Induced Fluorescence

We used laser-induced fluorescence (LIF) extensively in this study as a diagnostic technique, as it has been applied widely in Hall thruster research.[19] This system involves injecting laser light into the plasma at a specific wavelength λ detuned slightly from a metastable transition wavelength λ_0. Due to the Doppler effect, particles moving at a certain velocity will see the detuned laser shifted to the transition wavelength, and thus will excite and fluoresce spontaneously. This fluorescence is collected and its intensity serves as a measure of the density of particles moving at that velocity. The precise relationship between velocity and wavelength, for the speed of light in vacuum c, is given by

$$u_i = c\frac{\lambda - \lambda_0}{\lambda_0} \quad . \tag{3}$$

In this study, both Xe II and Xe I transitions were targeted to probe the velocity distributions of ions and neutrals. Both schemes are non-resonant and excite metastable particles, and so it must be assumed that the metastable response is indicative of the ground state response. In particular, the Xe II $5d[4]_{7/2}$–$6p[3]_{5/2}$ (834.953 nm) and Xe I $6s^2[1/2]_1^0$–$6p^2[3/2]_2$ (834.912 nm) transitions were used. In short, the LIF hardware begins with the laser and tapered amplifier, which emit a beam that is sampled by a wavemeter and photodiode. The beam is split and chopped and fiber-coupled into the vacuum chamber. The collected light is filtered with a set of dielectric layer bandpass filters that isolate it to the expected wavelength ±4 nm, and shone into a photomultiplier tube. The photocurrent is transduced with a transimpedance amplifier and homodyned with a lock-in amplifier. A more complete description of this setup is provided in Ref. 20.

In this experiment, the thruster was mounted on an axial motion stage to allow us to interrogate different locations in the plasma. However, the range of motion was mostly limited by the strength of the fluorescence signal. As a result, Xe II data was acquired from a z/L (axial position normalized by channel length) of 0 to 0.66, representing a region extending from the exit plane and downstream into the near plume. For Xe I LIF, we probed from z/L -0.26 to -0.99, representing a region extending from behind the exit plane upstream to the anode.

C. Electrostatic Probe

An electrostatic probe was also used to provide an ion current density boundary condition for the LIF data collected in this experiment. This Faraday probe consisted of a 4-mm diameter tungsten collector housed in an alumina tube, itself wrapped in a foil guard electrode. A photo of the probe tip is included as Fig. 2. In operation, the Faraday probe was biased to -30 V and its current measured with a picoammeter. The probe radially strafed the thruster at axial distances ranging from 10 to 100 cm using a fast linear motor.

Fig. 2 The tip of the Faraday probe.

D. Boltzmann Moment Analysis

From the aforementioned diagnostics, the velocity moments of the ions and neutrals are measured, as well as the plasma density at the Faraday probe location via the relation $n = j_i/(eu_i)$. What remains to be determined are f_{iz}, E_z, n_n, and n (everywhere). To do this, moments of the one-dimensional Boltzmann equation for ions are solved explicitly as a system of equations to yield f_{iz}, E_z, and the characteristic plasma density gradient frequency $f_n \equiv u_i(dn/dz)/n$. The details of this approach are described thoroughly in Ref. 21, and it is based on work by Pérez-Luna et al.[22] As a quick summary, the equations being solved are

$$\frac{\partial n}{\partial t} + \frac{\partial \overline{u} n}{\partial z} = n f_{iz} \quad , \tag{4}$$

$$\frac{\partial \overline{u} n}{\partial t} + \frac{\partial \overline{u^2} n}{\partial z} - \frac{e}{m} n E_z = 0 \quad , \tag{5}$$

and

$$\frac{\partial \overline{u^2} n}{\partial t} + \frac{\partial \overline{u^3} n}{\partial z} - 2\frac{e}{m} n E_z \overline{u} = 3\frac{e}{m} T_i n f_{iz} \quad , \tag{6}$$

where the j$^{\text{th}}$ moment is conveyed $\overline{u^j}$, and T_i is the temperature of newborn ions. An explicit solution for this system is found as follows, where it is assumed T_i is small compared to the kinetic energy of the ions:

$$f_{iz} = \frac{-\overline{u_i}\frac{dD}{dz} + N}{D} \quad \text{where} \quad D = 2\overline{u_i}\,\overline{u_i^2} - \overline{u_i^3} \quad \text{and} \quad N = \frac{d\overline{u_i}}{dz}(2\overline{u_i}\,\overline{u_i^2} + D) \quad , \tag{7}$$

$$E_z = \frac{m_i}{e}\left(M + \frac{\overline{u_i^2} f_{iz}}{\overline{u_i}}\right) \quad \text{where} \quad M = \frac{d\overline{u_i^2}}{dz} - \frac{d\overline{u_i}}{dz}\frac{\overline{u_i^2}}{\overline{u_i}} \quad , \tag{8}$$

and

$$f_n = \frac{d\overline{u_i}}{dz} - f_{iz} \quad . \tag{9}$$

From this information, $n \propto \exp[\int(-f_n/u_i)dz]$ where the constant of proportionality is determined by the boundary density measurements, in this case made with the Faraday probe.

Because the Xe I and Xe II LIF interrogation domains do not overlap, there are not sufficient boundary conditions to take a similar approach for the neutral gas. However, using the LIF measurements of u_n and far-field ionization gauge readings to inform an approximate neutral speed downstream of the exit plane, the neutral continuity equation can simply yield n_n:

$$n_n \propto \exp\left[\int \frac{-nf_{iz}}{u_n}dz\right] \quad , \tag{10}$$

where we assume du_n/dz is small, and the constant of proportionality comes from a downstream estimate of n_n. This boundary condition is derived from a continuity argument assuming a Lorentzian plasma current density distribution downstream and little divergence in the near plume. With these analysis techniques, the remaining quantities f_{iz}, E_z, n_n, and n can be determined. As a result, a combination of LIF, in situ electrostatic probing, and a Boltzmann moment analysis can yield all the parameters needed to assess the frequency scaling of the theories outlined in Section II.

IV. Results

We show in this section the measurements of the plasma properties necessary to evaluate the three proposed theories for the breathing mode. These include the discharge current waveforms, collected as part of the typical thruster telemetry; the Faraday probe data, acquired at different axial locations; the LIF data for both ions and neutrals; and finally the quantities inferred with the Boltzmann analysis.

A. Probe Results

Figure 3 shows a discharge current spectrum for the nominal 7% CFF condition, as well as the variation in peak frequency and spectral width with CFF. The breathing peak in the spectra tended to be triangular, which implies the waveform has a cnoidal shape. However, as the breathing frequency decreases the spectral width also decreases, indicating that the waveform is broadening toward a sine-like shape.

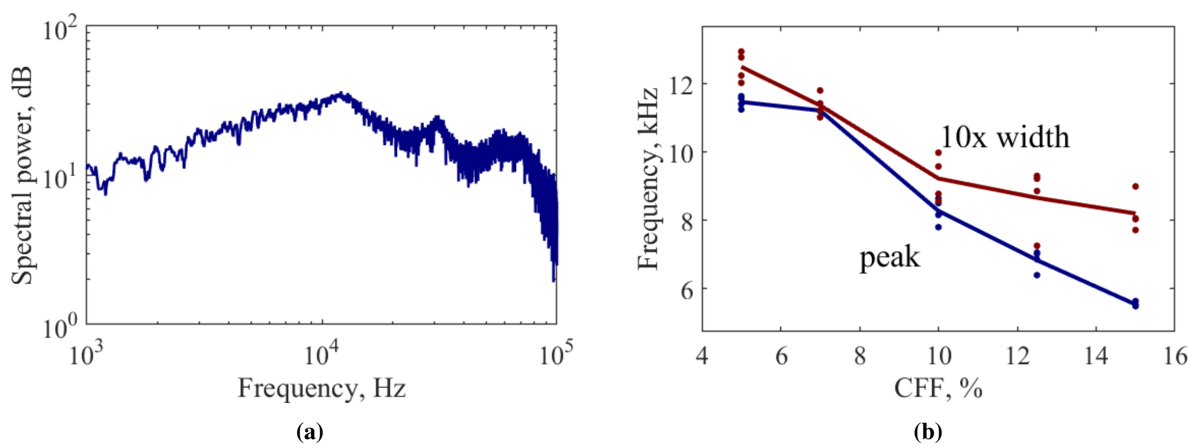

Fig. 3 The nominal discharge current spectrum (a) and the variation of peak frequency (blue) and width (red) with CFF (b).

Figure 4 shows the ion current density j_i on channel centerline as a function of axial position, as well as an extrapolation to the most downstream LIF acquisition point. The extrapolation is performed assuming a z^{-2} scaling, which comes from the physical interpretation that the beam expands conically. The extrapolated value is found to be 124 mA/cm^2. The "anode limit" – that is, the nominal uniform discharge current density at the anode – is included for reference, where exceeding that limits implies that current is concentrated on channel centerline.

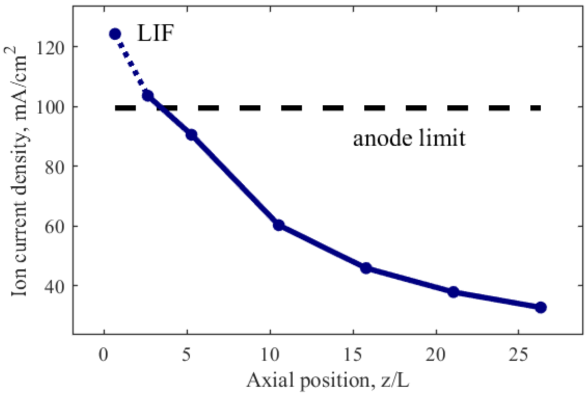

Fig. 4 The ion current density measured with the Faraday probe as a function of axial position.

Figure 5 shows the mean velocities for ions and neutrals as measured with LIF. The profiles for a few different CFF conditions are shown. It appears that the ion velocity increases almost uniformly as CFF increases, while a trend in the neutral profiles is harder to discern. The shift in the ion profiles agrees with a previous study that concluded the changes in neutral density as a result of varying the CFF are responsible for shifts in the acceleration region location.[23]

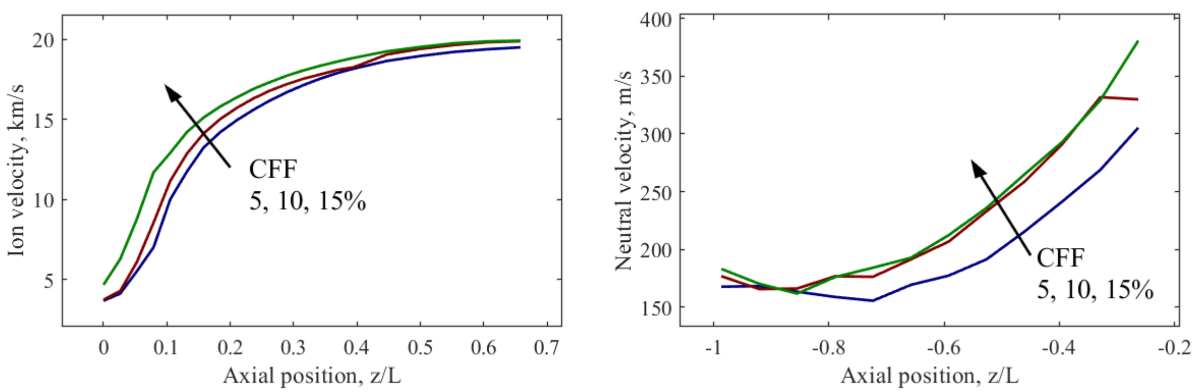

(a) **(b)**

Fig. 5 Mean velocity profiles for ions (a) and neutrals (b) for a few different CFFs.

The result of applying the method of Section III.D is shown for 5%, 10%, and 15% CFF in Fig. 7. As CFF increases, the location of peak f_{iz} and E_z both shift upstream, and a somewhat similar trend is apparent in f_n. Similarly, f_{iz} and E_z become narrower but taller with increasing CFF. Using the LIF, Faraday probe, and ionization gauge measurements together, downstream boundaries for n and n_n, found to be 3.9×10^{17} and 1.4×10^{18} m^{-3} respectively, permit both density profiles to be inferred. The computed density profiles are shown for the same CFFs in Fig. 6. The neutral density profiles are included merely for the sake of comparison; they are not used in any further analyses and we expect them to be slightly inaccurate since they do not account for the additional gas influx from the cathode, which is a function of CFF.

B. Correlation Study

We now use the measurements of all the fundamental parameters described in Section II to test the frequency scaling relationship dictated by the predator-prey, resistive instability, and neutral gas instability models. To reiterate Section II, the correlation between the calculated and observed frequencies, f and f_0, is used to indicate whether a theory is physically accurate. Specifically, we examine the correlation coefficient r, defined as the ratio of the covariance of the

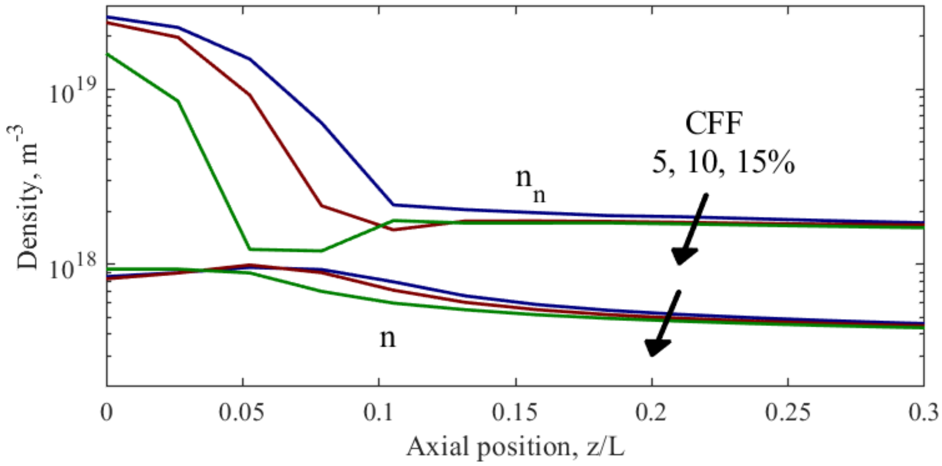

Fig. 6 The ion and neutral density profiles for a few CFFs.

two frequencies to the product of their standard deviations

$$r = \frac{\sum(f - \overline{f})\sum(f_0 - \overline{f_0})}{\sigma\sigma_0} \ , \tag{11}$$

where the sums are over all samples of f or f_0. As an example, when $f = f_0$ such that there is perfect correlation, the numerator of Eq. (12) becomes ${\sigma_0}^2$; since $\sigma = \sigma_0$ in this case, the correlation coefficient is therefore 1. In general, r can be: positive, suggesting a theory is accurate; negative, indicating a theory is inaccurate; or near zero, suggesting the instability was absent or the measurements were too insensitive. We also consider the p-value of the correlation,

$$p = 2\int_t^\infty \frac{\Gamma\left(\frac{N}{2}\right)}{\sqrt{\pi(N-1)}\Gamma\left(\frac{N-1}{2}\right)}\left[1 + \frac{x^2}{N-1}\right]^{-\frac{N}{2}} dx \quad \text{for} \quad t = \frac{\overline{f - f_0}}{\sigma} \ , \tag{12}$$

where x is the integration variable, Γ is the gamma function, and N is the number of samples of f and f_0. This quantity represents the probability of observing the same correlation by random chance according to a t-distribution. In this study the standard 5% significance level is used, below which any correlation cannot be rejected. We acknowledge that performing these analyses on such small data sets – only five CFF conditions were tested, as shown in Fig. 3 – reduces the meaningfulness of t-testing, but we proceed with it here as a measure of correlation, even if it does not represent the statistically-rigorous correlation.

1. Predator-Prey

To evaluate the frequency scaling of Eq. (1), realistic choices for u_i, u_n, and L must first be made. For L, the characteristic length of the plasma discharge, we consider two possible and physically reasonable definitions: the total channel length and the length of the combined ionization-acceleration region. Figure 8a shows both the ionization and acceleration regions as measured with the LIF technique described in Section III. Displayed are the mean location of f_{iz} (which tends to coincide with the peak in f_{iz}), z_{iz}, and the range between the peak in E_z and its mean location z_{acc}. Note that the two regions are quite close together relative to the extent of the acceleration region. The region widths w_{iz} and w_{acc} were calculated as the integral half-width of f_{iz} and E_z about their peak values; an example is shown in Fig. 8b for the 7% CFF condition. In practice, we define the combined ionization-acceleration region to extend from $\overline{z_{iz}} - w_{iz}/2$ to $\overline{z_{acc}} + w_{acc}/2$.

Using these definitions, Eq. (1) can be compared to the observed breathing frequency. This is shown in Fig. 9 where L is the channel length ("long") and the ionization-acceleration region length ("short"). Also included is a dashed line of perfect correlation. The calculated magnitudes for the "long" case are nearly reasonable but for "short" they are an order of magnitude too large. The correlation coefficients are -0.65 and -0.88 with null probabilities of 23% and 4.6%, respectively. This means that using the channel length yields weak and negative correlation while using

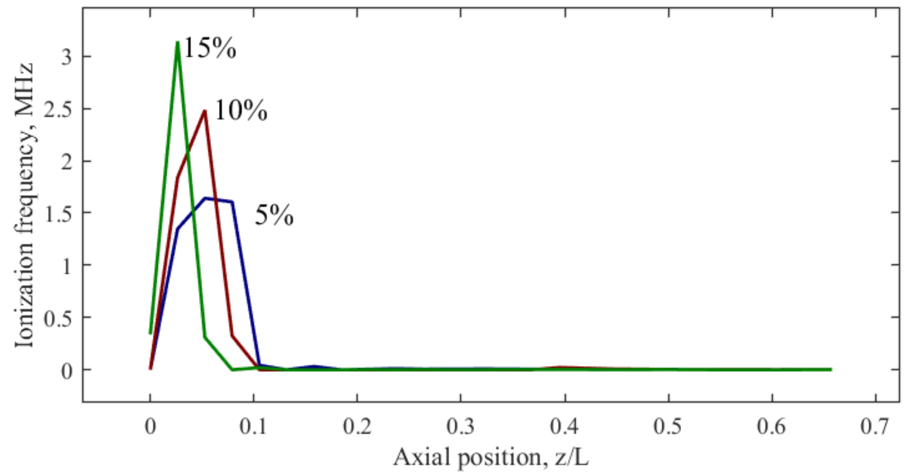

(a)

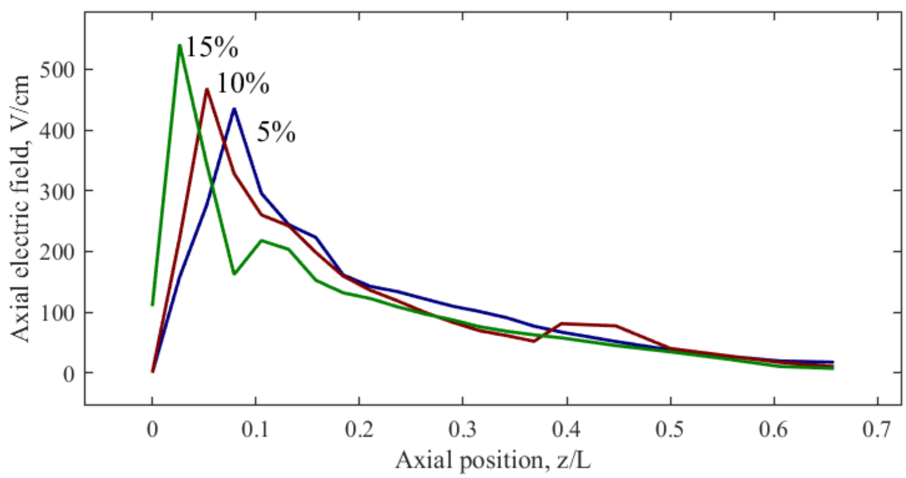

(b)

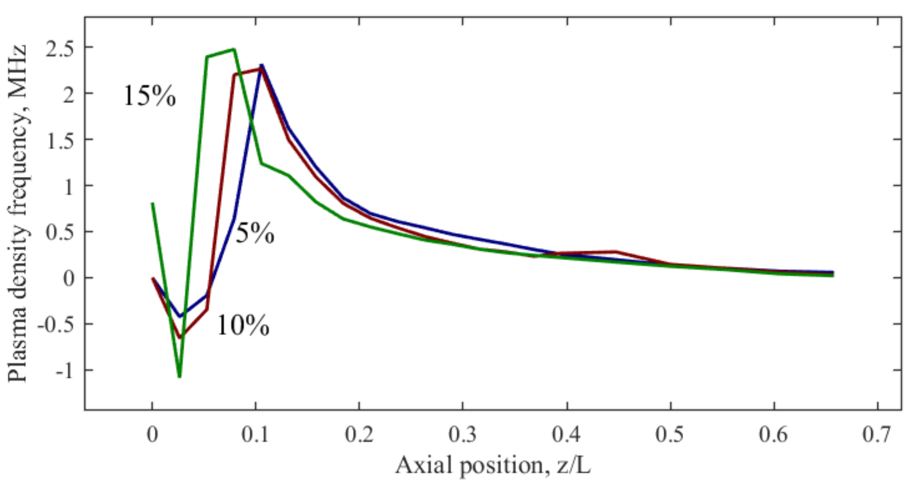

(c)

Fig. 7 The quantities determined from the Boltzmann moment analysis, including ionization frequency (a), axial electric field strength (b), and plasma density frequency (c) for a few CFFs.

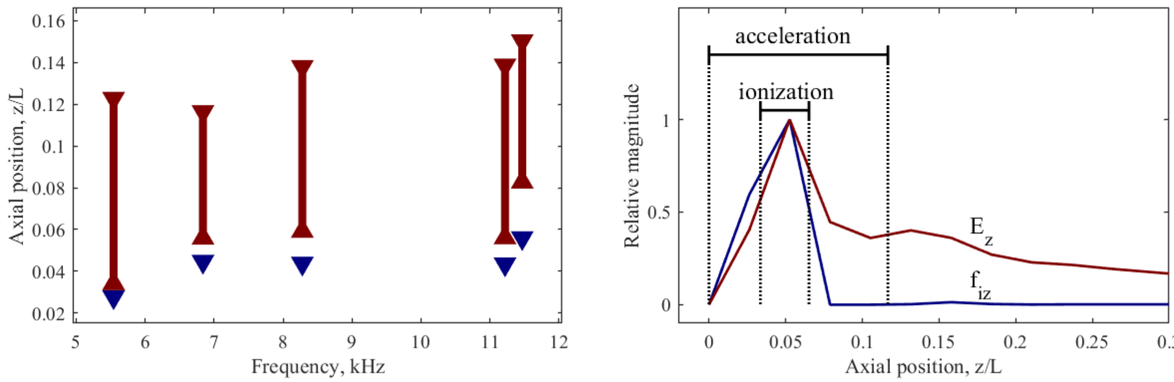

(a) **(b)**

Fig. 8 (a) The ionization and acceleration regions, where in the latter the location of peak E_z and mean E_z are delineated. (b) An example of determining the width of the ionization and acceleration regions, here for the 7% CFF condition.

the ionization-acceleration region length yields strong and negative correlation, where the latter may be statistically insignificant. In total, this suggests that the frequency scaling dictated by the predator-prey model is inconsistent with the experimental data.

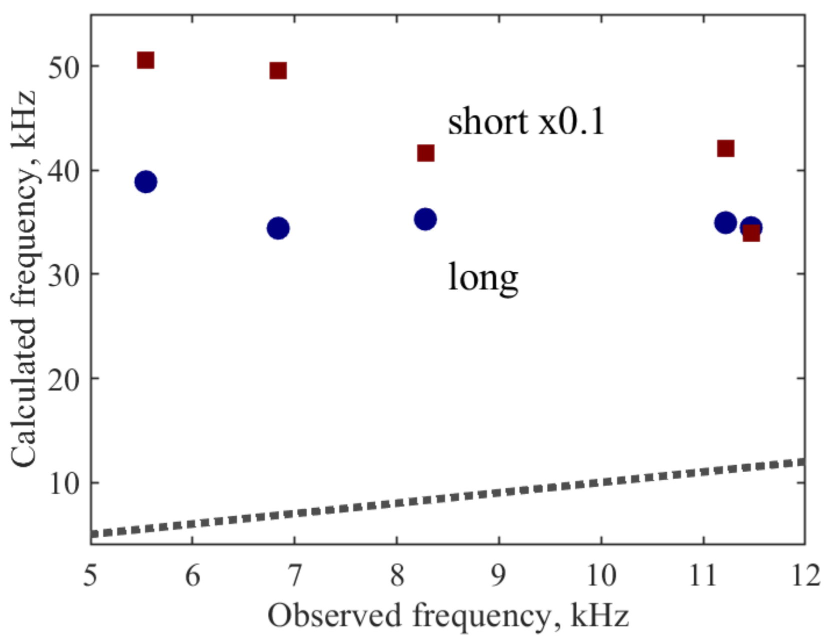

Fig. 9 A comparison of the frequency predicted with the predator-prey model using a long and short length scale.

2. Resistive Instability

Unlike the predator-prey model, the dispersion for the resistive instability has a spatial dependence such that it is sensible to evaluate Eq. (2) at all points throughout the measured domain. Figure 10a shows the growth rate predicted by this model for a few CFF conditions. It indicates that the growth peaks in the near plume, weakening farther downstream and in the ionization/acceleration region. This is in agreement with Chables and Rogier's assessment that this mode should stabilize when electron mobility is very high (downstream) or very low (upstream). Instead of comparing the real part of Eq. (2) to the breathing frequency, we argue that it is more physically meaningful to examine correlation with the growth rate of the resistive instability. This is because, as Chables and Rogier implied in their work, the resistive instability only drives ionization oscillations but the breathing process occurs much slower. We propose here though that the growth rate of the resistive instability does in some way dictate the breathing frequency: if the resistive instability grows quickly, predator-prey-like thickening of the plasma and depletion of neutrals can occur faster. Figure 10b shows the relative peak growth rate of the resistive instability as a function of the observed breathing frequencies. As Fig. 10a indicates, the growth rates tend to be much higher than the measured breathing frequencies, so in Fig. 10b they have been normalized to the mean breathing frequency, and a line of perfect correlation has been included. There is little correlation between the growth rate and the breathing frequency. In fact, the null probability is calculated to be 95%, which indicates that it is highly likely that any correlation measured is spurious. This suggests that the resistive instability, although potentially supported in a Hall thruster, likely does not set the pace of breathing oscillations.

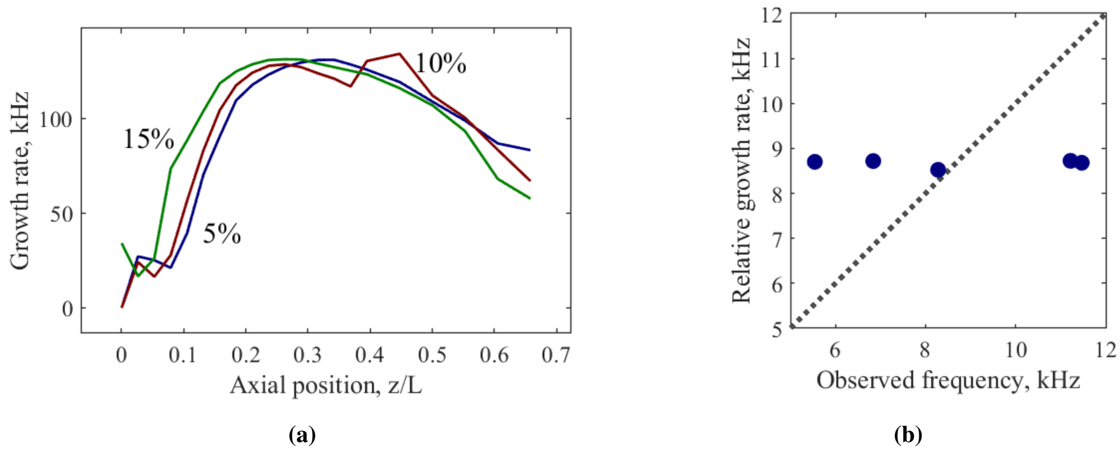

Fig. 10 The growth rate (a) and normalized peak growth rate vs breathing frequency (b) for the resistive mode. A line of perfect correlation is shown in the second plot for reference.

3. Neutral Gas Instability

Determining the viability of a neutral gas instability as an explanation of the breathing mode is difficult because there is no quantitative theory for comparison with the experimental data. However, there are a few neutral properties that can be examined. Figure 11a shows the neutral transit frequency from anode to ionization region compared to the observed breathing frequency. Also included are estimates of the bounds of this curve due to the fact that the Xe I LIF data does not extend to the ionization region. Regardless, the plot shows that the correlation is negative but the frequencies are the correct order of magnitude. Figure 11b shows the acoustic frequency for continuum neutral sound waves compared to the observed breathing frequency, with bounding curves as in Fig. 11a. Again the magnitudes are nearly correct but here the correlation is conceivably positive.

At first glance, this is an encouraging result: the breathing behavior observed experimentally is described well by a neutral acoustic wave traveling from the anode to the ionization region. However, there are several factors that temper this conclusion. First, because the gas is rarefied the sound speed will actually be somewhat higher than considered here, which will drive the frequencies even lower than they are already. This is intuitive: in the limit of a single-particle gas, there is no change in phase of an acoustic perturbation because there is no interaction between particles, and thus the sound speed is apparently infinite. Second, even though the correlation is positive, the neutral acoustic frequency actually changes very little, 150 Hz, compared to the observed change of about 6 kHz. The small change in frequency in both plots of Fig. 11 is in fact evidence that the neutral gas was relatively insensitive to changes in breathing frequency. Finally, there is a physical inconsistency with a neutral acoustic-driven breathing mechanism. Such an instability might involve shocks being thrown off the anode periodically and traveling toward the ionization region. In that case, the frequency of any plasma oscillations should be set by this shock-throwing process, not by the transit rate of the shocks. The only way that this physical picture could could be reconciled with the experimental data is if there is coupling

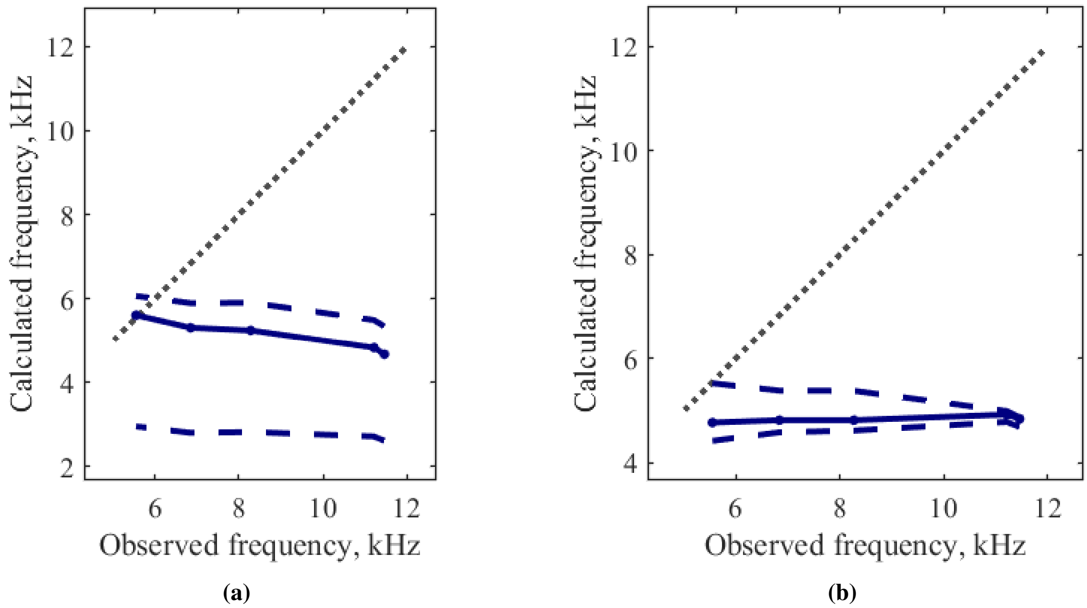

Fig. 11 The calculated neutral transit frequency (a) and acoustic frequency (b) compared to the observed frequency. The dashed bounding curves account for the fact that Xe I LIF was not performed all the way to the ionization region.

between the process at the anode generating the waves and the downstream plasma. This might involve a plasma wave or neutral shock traveling between the two regions.

V. Discussion

A. Shortcomings

Although we have established that the three theories considered in this paper all fail to accurately describe the breathing mode, it is important to speculate why this is so. It is possible that some of these processes, like the resistive instability, actually do exist in Hall thrusters, but detecting them was not within the scope of this study. Therefore, our goal is not to determine why these instabilities are unphysical but simply why they are not responsible for low-frequency breathing oscillations.

1. Predator-Prey

The predator-prey model presents a relatively simple physical picture and so determining its limitations is also straightforward. As the measured breathing frequency increases, the discharge moves outward slightly, as shown in Fig. 8a. Although the mean ion velocity profiles also shift according to Fig. 5, u_i at the location of mean E_z varies by only about 11%. Further, Fig. 5 also showed that u_n appeared largely insensitive to changes in CFF. Finally, the size of the ionization-acceleration region increases slightly with frequency, as shown in Fig. 8a. As a result, u_i and u_n both vary little, and $1/L$ either decreases with frequency or does not change if L is taken to be the channel length. It is unsurprising then that Eq. (1) does not match the measured frequency trend. Physically, the predator-prey model assumes that the transit time of neutrals and ions dictates the breathing frequency, but in this study we find that those times vary little.

2. Resistive Instability

The discrepancy between the measured breathing behavior and the predictions of Eq. (2) is harder to determine since that dispersion relation predicts growth of the instability. Assuming $\delta \ll 1$, it can be demonstrated that

$$\omega_r \propto 1 \pm \frac{1}{2\delta} \quad \text{and} \quad \gamma \propto -\frac{1}{2} \pm \frac{1}{4\delta}. \tag{13}$$

Figure 7 shows that E_z decreases with breathing frequency, while Fig. 6 shows that n increases with breathing frequency. Given the method to calculate μ_e outlined in Section III, a decreasing E_z will increase μ_e but an increasing n will decrease μ_e. Together, these trends make μ_e insensitive to ω_b such that δ changes very little with frequency. And as borne out in Fig. 10b, this results in a high null probability. Physically, the resistive mode relies on a two-stream instability so it depends strongly on u_i and μ_e. However, the experimental data shows that both of these quantities vary weakly with changes in the breathing frequency.

3. Neutral Gas Instability

Unlike the other two theories, the neutral transit frequencies are markedly close to the observed breathing frequencies. The fundamental issue here is that the ionization region pushes outward as the breathing frequency increases, which lengthens the transit time given that u_n changes little. This trend is reversed in Fig. 11b because the neutral gas gets slightly hotter with increasing ω_b. Ultimately, a neutral-driven instability would need to rely on a different length scale to correspond with the breathing mode.

However, a larger discrepancy also exists. The transit time across the Xe I LIF domain – informed completely by direct measurements with minimal assumptions – can be up to 68% *greater* than the observed breathing period. This is disconcerting because Xe I LIF was only performed up to $0.75L$ while the ionization-acceleration zone is closer to $1.1L$ on average. In effect, the most reliable measurement of neutral transit time from the anode does not even extend to the ionization region yet is still too long to be consistent with the breathing mode. This is evidence that the neutral transit time cannot by itself capture real trends in ω_b.

B. Alternatives

C. Analytical Limitations

Before examining an alternative physical mechanism to explain the trends experimentally observed in this study, it is important to evaluate the limitations of the findings of the previous sections. One egregious problem is estimating correlation with only five data points – the five CFF conditions – available for comparison. With so few data points, it is expected that p-values will always be high, which will almost always render the conclusion that a lack of correlation cannot be rejected. For the purposes of this study, such a result would be unproductive. However, as exemplified by Fig. **??** there were many instances were the null probability was quite low, even below 5%. This means that in some cases a negative correlation could not be rejected, which gives confidence that the t-testing was still meaningful.

Further, even if the p-values could not be trusted, the scarcity of positive correlation with any of the three hypotheses examined is in itself compelling evidence that none of them accurately describe the breathing mode. For the predator-prey model, Fig. 9 demonstrates there is either no or weak correlation, regardless of the computed statistical significance. For the resistive instability, positive correlation was associated with low growth, and even then the high-growth real frequencies are much too high. For the neutral gas instability, any positive correlation is weak and the real frequencies are slightly too small. In total, the calculation of low p-values in some cases and the lack of positive correlation both instill confidence that the results of the previous sections are reliable.

1. Possible Mechanism

If the analyses so far are to be trusted, there must be an alternative mechanism governing the breathing mode. The shortcoming of all the theories considered in this study is primarily that their dependence on quantities insensitive to CFF like u_i, u_n, and μ_e is too strong compared to other parameters like L. Leveraging these findings to provide an alternative description of the breathing mode, we can either assume that quantities like u_i, u_n, or μ_e are irrelevant, or we can assume that the regions we have examined are irrelevant. For example, u_i may show poor correlation with ω_b in the near plume but may correlate much better in the acceleration region; a theory involving the near plume will fail to describe ω_b while one involving the acceleration region will succeed, despite both depending on u_i. Although a thorough investigation of this possibility is reserved for future work, a cursory examination of the correlation of u_n with ω_b is conducted and displayed in Fig. 12. The null probability tends to be low everywhere while the correlation coefficient is generally large, with a minimum of the former occurring at z/L=-0.72.

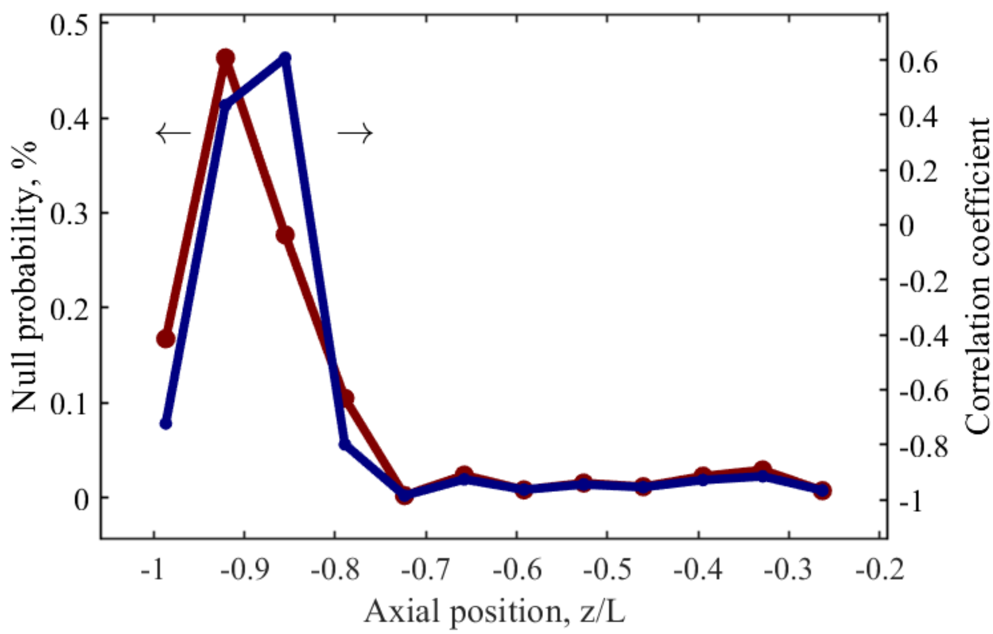

Fig. 12 The correlation coefficient and null probability of the neutral velocity and breathing frequency as function of axial position.

One possibility presented by Fig. 12 is that the neutral behavior in the anode-to-exit plane region may impact low-frequency oscillations. As f_{iz} is generally small here, there may be some other plasma process affecting the neutral population in this region. In that sense, it is possible that the neutral dynamics upstream of the exit plane are significant. Although we expect the electron exit plane-to-anode transit period to be much shorter than the breathing mode – anywhere from $O(1)$ to $O(10)$ μs – electrons may still play role in determining ω_b.

VI. Conclusions

In summary, an experimental validation of proposed breathing mode mechanisms is needed to improve understanding of these low-frequency oscillations, thereby helping to predict and potentially mitigate operational consequences associated with this mode. A combination of laser-induced fluorescence, electrostatic probing, and an analysis of Boltzmann equation moments allowed access to the plasma parameters needed to test three distinct breathing theories. The predator-prey description yielded frequencies that differed from experimental measurements in both magnitude and trend. The resistive model did predict regions that matched the trend of the observed frequencies, but it also attributed low growth to these regions and the correlation was still statistically insignificant. Finally, a neutral-driven mechanism was explored and it was found that the neutral transit frequency and neutral acoustic frequency both agreed well in terms of magnitude. The trend of the former was inconsistent with experimental observations but that of the latter was in fact consistent. However, the physical discrepancies and assumptions made for predicting the neutral sound speed render this finding suspect. In total, of the three breathing mode models examined, none were found to agree with experimental data. This highlights the need for further study of the breathing mode, and to this end we have performed a brief correlational study of neutral velocity that shows the region near the anode may play an active role in breathing oscillations. By refuting three hypotheses and providing insight for formulating a new description of the breathing mode, this work has advanced the understanding of this instability and thereby represents a step forward in predicting the stability of Hall thrusters in general.

References

[1] Oh, D. Y., Snyder, J. S., Goebel, D. M., Hofer, R. R., and Randolph, T. M., "Solar Electric Propulsion for Discovery-Class Missions," *Journal of Spacecraft and Rockets*, Vol. 51, No. 6, 2014, pp. 1822–1835. doi:10.2514/1.A32889, URL `https://doi.org/10.2514/1.A32889`.

[2] Choueiri, E. Y., "Plasma oscillations in Hall thrusters," *Physics of Plasmas (1994-present)*, Vol. 8, No. 4, 2001, pp. 1411–1426. doi:10.1063/1.1354644, URL `http://scitation.aip.org/content/aip/journal/pop/8/4/10.1063/1.1354644`.

[3] Sekerak, M. J., Gallimore, A. D., Brown, D. L., Hofer, R. R., and Polk, J. E., "Mode Transitions in Hall-Effect Thrusters Induced by Variable Magnetic Field Strength," *Journal of Propulsion and Power*, Vol. 32, No. 4, 2016, pp. 903–917. doi:10.2514/1.B35709, URL `http://dx.doi.org/10.2514/1.B35709`.

[4] Ortega, A. L., Mikellides, I. G., and Chaplin, V. H., "Numerical Simulations for the Assessment of Erosion in the 12.5-kW Hall Effect Rocket with Magnetic Shielding (HERMeS)," *35th International Electric Propulsion Conference, Atlanta, GA, IEPC-2017-154*, 2017.

[5] Fife, J., Martinez-Sanchez, M., and Szabo, J., "A numerical study of low-frequency discharge oscillations in Hall thrusters," *33rd AIAA/ASME/SAE/ASEE Joint Propulsion Conference and Exhibit*, American Institute of Aeronautics and Astronautics, 1997. doi:10.2514/6.1997-3052, URL `http://arc.aiaa.org/doi/10.2514/6.1997-3052`.

[6] Chable, S., and Rogier, F., "Numerical investigation and modeling of stationary plasma thruster low frequency oscillations," *Physics of Plasmas*, Vol. 12, No. 3, 2005. doi:10.1063/1.1857913, URL `http://aip.scitation.org.proxy.lib.umich.edu/doi/10.1063/1.1857913`.

[7] Barral, S., and Peradzyński, Z., "Ionization oscillations in Hall accelerators," *Physics of Plasmas (1994-present)*, Vol. 17, No. 1, 2010. doi:10.1063/1.3292645, URL `http://scitation.aip.org/content/aip/journal/pop/17/1/10.1063/1.3292645`.

[8] Hara, K., Sekerak, M. J., Boyd, I. D., and Gallimore, A. D., "Perturbation analysis of ionization oscillations in Hall effect thrusters," *Physics of Plasmas (1994-present)*, Vol. 21, No. 12, 2014. doi:10.1063/1.4903843, URL `http://scitation.aip.org/content/aip/journal/pop/21/12/10.1063/1.4903843`.

[9] Litvak, A. A., and Fisch, N. J., "Resistive instabilities in Hall current plasma discharge," *Physics of Plasmas*, Vol. 8, No. 2, 2001, pp. 648–651. doi:10.1063/1.1336531, URL `http://aip.scitation.org/doi/abs/10.1063/1.1336531`.

[10] Koshkarov, O., Smolyakov, A. I., Romadanov, I. V., Chapurin, O., Umansky, M. V., Raitses, Y., and Kaganovich, I. D., "Current flow instability and nonlinear structures in dissipative two-fluid plasmas," *Physics of Plasmas*, Vol. 25, No. 1, 2018, p. 011604. doi:10.1063/1.5017521, URL `http://aip.scitation.org/doi/10.1063/1.5017521`.

[11] Mazouffre, S., Bourgeois, G., Garrigues, L., and Pawelec, E., "A comprehensive study on the atom flow in the cross-field discharge of a Hall thruster," *Journal of Physics D: Applied Physics*, Vol. 44, No. 10, 2011, p. 105203. doi:10.1088/0022-3727/44/10/105203, URL `http://stacks.iop.org/0022-3727/44/i=10/a=105203`.

[12] Hara, K., and Mikellides, I. G., "Characterization of low frequency ionization oscillations in Hall thrusters using a one-dimensional fluid model," American Institute of Aeronautics and Astronautics, Cincinnati, Ohio, 2018. doi:10.2514/6.2018-4904, URL `https://arc.aiaa.org/doi/10.2514/6.2018-4904`.

[13] Lucca Fabris, A., Young, C. V., and Cappelli, M. A., "Time-resolved laser-induced fluorescence measurement of ion and neutral dynamics in a Hall thruster during ionization oscillations," *Journal of Applied Physics*, Vol. 118, No. 23, 2015. doi:10.1063/1.4937272, URL `http://aip.scitation.org/doi/full/10.1063/1.4937272`.

[14] Rayleigh, L., *The Theory of Sound*, Vol. 1, Macmillan, London, 1877. URL `https://www.irphe.fr/~clanet/otherpaperfile/articles/Rayleigh/N0095130_PDF_1_340.pdf`.

[15] Reid, B. M., "The Influence of Neutral Flow Rate in the Operation of Hall Thrusters," Ph.D., University of Michigan, Ann Arbor, MI, 2009.

[16] Hofer, R., Cusson, S., Lobbia, R., and Gallimore, A., "The H9 Magnetically Shielded Hall Thruster," *35th International Electric Propulsion Conference*, Vol. IEPC- 2017- 232, 2017.

[17] Cusson, S., Hofer, R., Lobbia, R., Jorns, B., and Gallimore, A., "Performance of the H9 Magnetically Shielded Hall Thrusters," *35th International Electric Propulsion Conference*, Vol. IEPC-2017-239, 2017.

[18] Dankanich, J. W., Walker, M., Swiatek, M. W., and Yim, J. T., "Recommended Practice for Pressure Measurement and Calculation of Effective Pumping Speed in Electric Propulsion Testing," *Journal of Propulsion and Power*, Vol. 33, No. 3, 2017, pp. 668–680. doi:10.2514/1.B35478, URL https://arc.aiaa.org/doi/10.2514/1.B35478.

[19] Mazouffre, S., "Laser-induced fluorescence diagnostics of the cross-field discharge of Hall thrusters," *Plasma Sources Science and Technology*, Vol. 22, No. 1, 2013, p. 013001. doi:10.1088/0963-0252/22/1/013001, URL http://stacks.iop.org/0963-0252/22/i=1/a=013001.

[20] Dale, E., Gallimore, A., and Lobbia, R., "Time-resolved internal Hall thruster plasma measurements using a high-speed Langmuir probe," Phoenix, AZ, 2016.

[21] Dale, E. T., and Jorns, B. A., "Non-invasive time-resolved measurements of anomalous collision frequency in a Hall thruster," *Physics of Plasmas*, Vol. 26, No. 1, 2019, p. 013516. doi:10.1063/1.5077008, URL https://aip.scitation.org/doi/full/10.1063/1.5077008.

[22] Perez-Luna, J., Hagelaar, G. J. M., Garrigues, L., and Boeuf, J. P., "Method to obtain the electric field and the ionization frequency from laser induced fluorescence measurements," *Plasma Sources Science and Technology*, Vol. 18, No. 3, 2009, p. 034008. doi:10.1088/0963-0252/18/3/034008, URL http://stacks.iop.org/0963-0252/18/i=3/a=034008.

[23] Cusson, S. E., Dale, E. T., Jorns, B. A., and Gallimore, A. D., "Acceleration region dynamics in a magnetically shielded Hall thruster," *Physics of Plasmas*, Vol. 26, No. 2, 2019, p. 023506. doi:10.1063/1.5079414, URL https://aip.scitation.org/doi/10.1063/1.5079414.